

Combined Multiparametric X-Ray Diffraction Diagnostics of Microdefects in Silicon Crystals after Irradiation by High-Energy Electrons

E. N. Kislovskii^a, V. B. Molodkin^a, S. I. Olikhovskii^a, E. G. Len^a, B. V. Sheludchenko^a,
S. V. Lizunova^a, T. P. Vladimirova^a, E. V. Kochelab^a, O. V. Reshetnyk^a, V. V. Dovyanyuk^b,
I. M. Fodchuk^b, T. V. Lytvynchuk^b, and V. P. Klad'ko^c

^aKurdyumov Institute for Metal Physics, National Academy of Sciences of Ukraine, Kyiv, 03680 Ukraine

^bChernivsi National University, Chernivsi, 58012 Ukraine

^cLashkarev Institute for Semiconductor Physics, National Academy of Sciences of Ukraine, Kyiv, 03028 Ukraine

e-mail: yekis@imp.kiev.ua

Received September 18, 2012

Abstract—The quantitative diagnostics of complex defect structures in silicon crystals grown by the Czochralski method and irradiated with different doses of high-energy electrons (18 MeV) is performed by methods of high-resolution X-ray diffraction. The analysis is based on analytical formulas of the statistical dynamical theory of X-ray diffraction in nonideal crystals with randomly distributed defects of several types. Using the combined treatment of reciprocal space maps and rocking curves, the concentration and average radii of dislocation loops, as well as the concentration and radii of oxygen precipitates in the silicon samples, are determined.

DOI: 10.1134/S1027451013030270

INTRODUCTION

An understanding of changes in the structure and physical properties of silicon and other semiconductor materials under the action of irradiation by high-energy electrons is of considerable scientific and technological interest [1–5]. In particular, it opens up the possibility to purposefully influence structural changes and the associated mechanical, electrophysical, optical, and other properties of new developed functional materials.

Experimental studies into the generation and transformation of defects in silicon after electron irradiation are mainly devoted to intrinsic point defects and their complexes with dopant atoms. Such defects are studied using different spectroscopic methods [3–8]. Small clusters of intrinsic point defects and new phase particles in semiconductor crystals irradiated with electrons are also observed using transmission electron microscopy [8, 9] and differential X-ray diffractometry [10, 11].

Far fewer studies have been devoted to observing large growth microdefects in such crystals and to analysis of their interaction with primary radiation defects [12]. The corresponding investigations can be performed only by methods of high-resolution X-ray diffractometry using the results of the statistical dynamical theory of X-ray diffraction in nonideal crystals. The corresponding analytical results were obtained

recently in [13, 14] and provide a self-consistent description of the coherent and diffuse components of the diffraction intensity in crystals with several types of defects with arbitrary sizes.

The aim of this work is to apply high-resolution X-ray diffraction methods to determine changes in the concentration and sizes of the dominant types of microdefects in silicon single crystals grown by the Czochralski method (Cz-Si) after their irradiation with high-energy electrons.

BASIC EQUATIONS

Reciprocal Space Maps

The differential distributions of the intensity of X-ray diffraction measured on a three-crystal diffractometer (TCD) from nonideal crystals with randomly distributed defects consist of the sum of the coherent (I_{coh}) and diffuse (I_{diff}) components [15]. These components depend on the angular deviations $\Delta\theta$ and $\Delta\theta'$ of the studied crystal and analyzer crystal:

$$I(\Delta\theta, \Delta\theta') = I_{\text{coh}}(\Delta\theta, \Delta\theta') + I_{\text{diff}}(\Delta\theta, \Delta\theta'). \quad (1)$$

The coherent component of the two-dimensional intensity distribution measured using the TCD in the

case of quasi-dispersion-free geometry ($m, -n, m$) can be approximately represented in the form

$$I_{\text{coh}}(\Delta\theta, \Delta\theta') = I_0 \int_{-\infty}^{\infty} R_M \left(b_M^{-1} \left[b_S^{-1} (x - \Delta\theta) - \Delta\theta' \right] \right) \times R_{\text{coh}} \left(b_S^{-1} (x - \Delta\theta) \right) R_A(x - \Delta\theta) dx, \quad (2)$$

where I_0 is the intensity of the incident X-ray beam, R_M and R_A are the reflection coefficients of the monochromator crystal and analyzer crystal, and b_M and b_S are the parameters of asymmetry of the monochromator crystal and of the sample, respectively. The expressions for the coherent component of the reflection coefficient for a nonideal crystal with randomly distributed microdefects $R_{\text{coh}}(\Delta\theta)$ which were obtained somewhat earlier in [13, 16] take into account all effects of dynamical scattering, including the extinction of Bragg waves due to diffuse scattering (DS) at defects.

The diffuse component of the diffracted intensity measured using the TCD can be approximately represented by the following expression [15]:

$$I_{\text{diff}}(\Delta\theta, \Delta\theta') = I_0 \int_{-\infty}^{\infty} R_M(x) dx \int_{-\infty}^{\infty} r_{\text{diff}}(k_x, k_z) R_A(x' - \Delta\theta') dx', \quad (3)$$

$$r_{\text{diff}}(k_x, k_z) = K^{-1} \int R_D(\mathbf{k}) dk_y, \quad (4)$$

where $K = 2\pi/\lambda$ with λ being the X-ray radiation wavelength, and $R_D(\mathbf{k})$ is the diffuse component of the differential reflection coefficient. This component was calculated as a square of the dynamical diffuse scattering amplitude (the square is averaged over the random distribution of defects and integrated over the vertical divergence). The complex momentum transfer $\mathbf{q} = \mathbf{k} + i\mu_i \mathbf{n}$ that is contained in the expression for $R_D(\mathbf{k})$ in (4) includes the interference absorption coefficient μ_i . The vector \mathbf{k} describes the deviation from the of the reciprocal lattice point H . Its components k_x and k_z lie in the coherent scattering plane (\mathbf{K}, \mathbf{H}); the component k_z is directed along the inner normal $\mathbf{n} = \mathbf{e}_z$ to the crystal surface.

When several types of microdefects (α) are simultaneously present in a crystal with the size distribution (i), expression (4) should be merely replaced by a sum of corresponding expressions for each type of defects:

$$r_{\text{diff}}(k_x, k_z) = \sum_{\alpha} \sum_i r_{\text{diff}}^{\alpha i}(k_x, k_z). \quad (5)$$

Similarly, the exponent of the static Debye–Waller factor, in the absence of correlations in the position of defects, can be represented as the sum of contributions from each defect from the set $\{\alpha i\}$:

$$L_H = \sum_{\alpha} \sum_i L_H^{\alpha i}. \quad (6)$$

If the halfwidth of the function r_{diff} in (4) is significantly larger than the halfwidth of the reflection coefficients R_M and R_A , which usually takes place, these coefficients can be replaced by δ functions and expression (4) takes the form

$$I_{\text{diff}}(\Delta\theta, \Delta\theta') \approx I_0 R_{iM} R_{iA} r_{\text{diff}}(k_x, k_z). \quad (7)$$

where R_{iM} and R_{iA} are the integrated reflectivities of the monochromator and analyzer crystals, respectively.

In this work, reciprocal space maps and individual diffraction profiles are plotted using a TCD in the $\omega/2\theta$ scanning mode [17].

Rocking Curves

Measurements using the TCD in the ω scanning mode without an analyzer crystal provide the differential reflectivity of the studied sample integrated over the Ewald sphere, i.e., a rocking curve (RC). The diffuse component of the RC in the case of Bragg diffraction geometry in the thick crystal approximation can be written as [16]

$$R_{\text{diff}}(\Delta\theta) \approx F_{\text{dyn}}(\Delta\theta) \mu_{\text{HH}}(\Delta\theta) / (2\gamma_0 \mu_i). \quad (8)$$

Here, the factor $F_{\text{dyn}} \sim 1$ describes the angular modulation of the DS intensity caused by the dynamical interference of strong Bragg waves, and γ_0 is the direction cosine of the wave vector of the incident wave. The interference absorption coefficient μ_i is responsible for the extinction effects for diffusely scattered waves and can be estimated as $\mu_i \sim \pi/\Lambda$ in the total reflection range and $\mu_i \approx (1 + b)\mu_0/(2\gamma_0)$ beyond the range, respectively.

The dispersion corrections μ_{HH} due to DS in (8) are a sum of the coefficients of absorption due to DS for defects of the α type with the i th size $\mu_{\text{ds}}^{\alpha i}$:

$$\mu_{\text{HH}}(\Delta\theta) = \mu_{\text{ds}}(k_0) = \sum_{\alpha} \sum_i \mu_{\text{ds}}^{\alpha i}(k_0), \quad (9)$$

where $k_0 = K\Delta\theta \sin(2\theta_B)$, and θ_B is the Bragg angle. Expressions (8) and (9) describe both contributions from defects of several types to the DS intensity on the measured diffraction profiles and the absorption of the coherent component of scattering due to DS.

EXPERIMENT

The studied silicon samples with the (111) surface orientation and almost the same thickness ($t \approx 4.26$ mm) were cut from ingots grown by the Czochralski method, with the $\langle 111 \rangle$ growth axis. Two samples were irradiated with high-energy electrons (18 MeV) with doses of 1.8 and 3.6 kGy (Nos. 1A and 1B). The original sample No. 1 was used as the reference sample for comparison with the irradiated samples.

The reciprocal space maps of the samples were measured using a PANalytical X'Pert Pro MRD XL diffractometer for the symmetric Si (333) reflection (characteristic CuK_{α_1} radiation). Additionally, the

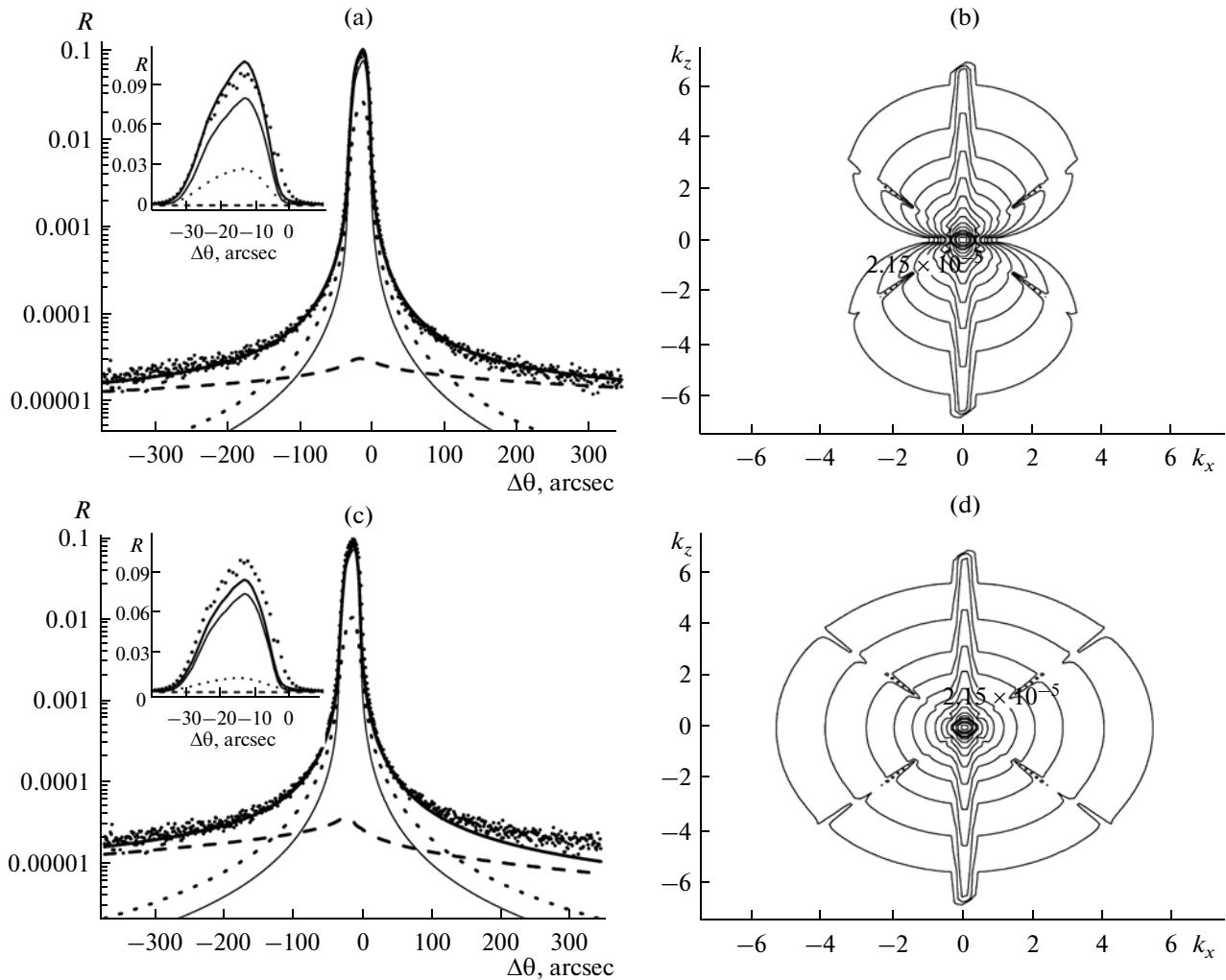


Fig. 1. (a, c) Experimental and theoretical RCs markers and thick solid lines, respectively; (b, d) calculated reciprocal space maps for the initial Cz-Si sample (No. 1); 333 reflection and $\text{CuK}\alpha_1$ radiation. The calculated RCs consist of a coherent component (thin solid line) and contributions to the DS intensity from large (dotted line) and small defects (dashed line). Figures 1a and 1b correspond to the presence of only spherical oxygen precipitates with two sizes; Figs. 1c and 1d, only to the presence of dislocation loops with two sizes.

RCs for the Si (333) reflection were measured in the ω scanning mode by using a TCD without the use of an analyzer crystal.

DIFFRACTION DATA TREATMENT AND DISCUSSION

When analyzing the measured diffraction profiles and reciprocal space maps, the contribution of thermal DS was neglected as a small quantity in the considered region of reciprocal space [16]. The influence of the instrumental function was taken into account when treating the RC and reciprocal space maps. At the same time, since the instrumental factors in treatment the diffusion component of the reciprocal space maps and their cross sections were taken into account approximately (see (7)), there are some discrepancies

between the theory and experiment. They are observed along the coherent peak from the sample, as well as in the form of extinction gaps on the calculated maps along the reciprocal space directions at which the Bragg condition is satisfied for wave vectors of the incident and diffusely scattered waves (Figs. 1–3). At the same time, the computation time was considerably decreased due to these simplifications.

The quality of RC fitting was determined by the ordinary and weighted reliability factors:

$$R = \sum_j |R_j^{\text{calc}} - R_j^{\text{meas}}| / \sum_j R_j^{\text{meas}},$$

$$R_w = (N + p)^{-1} \sum_j |R_j^{\text{calc}} - R_j^{\text{meas}}| / R_j^{\text{meas}}, \quad j = \overline{1, N}.$$

Here, R_j^{meas} and R_j^{calc} are the experimental and calculated reflectivities under the angular position of the sample $\Delta\theta_j$, N and p are the numbers of the experimental points and fitting parameters. The factors R and R_w are used for estimating the fitting quality in the total reflection range and for its uniform estimation in the entire measured angular range, respectively.

To perform detailed quantitative diagnostics of the studied Cz-Si crystals, it is necessary to choose an appropriate model of the defect structure. As a rule, for such crystals, the simultaneous presence of two types of randomly distributed microdefects can be supposed, namely, oxygen precipitates with different sizes and interstitial dislocation loops [18]. One of the main problems of the X-ray diffraction diagnostics of complex defect structures, that are also present in the studied samples, is the difficulty in identifying even two types of defects with similar (Coulomb type) asymptotic fields of static displacements that lead to such diffraction patterns. This problem manifests itself to an even larger extent when the DS intensity distribution is integrated over the Ewald sphere and, consequently, individual particularities of distributions from clusters and dislocation loops are smoothed. It is this case that takes place when the RCs are measured.

According to the analysis, neither the central and peripheral parts of the measured RCs nor of the reciprocal space maps can be described simultaneously for any of the studied samples using only one type of defects with a single size.

For this reason, the next step was to model the measured RCs using defects of one type with two significantly different effective radii, either of oxygen precipitates or of dislocation loops. It turned out (Fig. 1a) that the best RC fitting ($R = 11\%$ and $R_w = 9\%$) was reached in the presence of spherical precipitates with the following values of radii and concentrations in the crystal: $R_{p1} = 0.002 \mu\text{m}$, $n_{p1} = 1.1 \times 10^{17} \text{cm}^{-3}$, and $R_{p2} = 0.19 \mu\text{m}$, $n_{p2} = 2 \times 10^9 \text{cm}^{-3}$. However, according to calculations of the reciprocal space map with these defect parameters (Fig. 1b), it is impossible to describe the corresponding experimental map (Fig. 2a) using only precipitates because of the typical shape of the DS intensity distribution for these defects (the “double droplet”). Here, we note that all the maps are presented on a common scale and the intensities of neighboring isolines differ by a factor of $10^{1/3}$. The quantities k_x and k_z are presented in Figs. 1–3 in units of the reciprocal lattice parameter $d^{-1} \times 10^{-4}$.

The diffracted intensity distribution which is similar to that observed experimentally (Fig. 2) can be obtained under the assumption of the presence of dislocation loops with two sizes in the crystal (Fig. 1d). In this case, however, it is impossible to satisfactorily describe the central part of the RC (Fig. 1c; the minimal value of the reliability factor $R = 21\%$ is reached at $R_{L1} = 0.002 \mu\text{m}$, $n_{L1} = 1.1 \times 10^{16} \text{cm}^{-3}$ and $R_{L2} = 0.19 \mu\text{m}$, $n_{L2} = 2 \times 10^{11} \text{cm}^{-3}$). This difficulty is associ-

ated with the complex dynamical character of the interaction between the coherent and diffuse wave fields in a crystal with defects. Due to this interaction, the resulting diffraction pattern is determined not only by the effective radii of microdefects which specify the widths of the DS intensity distributions but also by the static Debye–Waller factor, as well as by the effect of extinction due to DS which significantly renormalize the contribution of the coherent component.

Similarly, one can demonstrate the inadequacy of the simultaneous fitting of RCs and maps when the crystal is assumed to have two types of defects (i.e., clusters and dislocation loops) each of which has only one size.

Thus, the simultaneous description of experimental RCs and reciprocal space maps turns out to be possible only when considering contributions from defects with at least three effective radii. As is seen from the foregoing analysis, on the one hand, the observed diffraction intensities in the region of total reflections for maps and RCs (Figs. 2–4) can be matched only by considering large spherical oxygen precipitates. On the other hand, the appropriate shape of the isolines on the maps can only be ensured with the dominant contribution of dislocation loops.

Therefore, it is necessary to emphasize the especially important role of the joint (combined) processing of maps and RCs for reliable quantitative determination of the microdefect characteristics with a wide spread in their effective sizes. Analyzing reciprocal space maps is the simplest way to unambiguously establish the dominant type of microdefects that make the main contribution to the measured differential DS intensity distributions and to determine the approximate characteristics of these defects. At the same time, owing to integration of the DS intensity over the Ewald sphere, rocking curves are more sensitive to small size defects as compared to maps in which the contribution of small defects is almost imperceptible.

Studying the reciprocal space maps for the initial (No. 1) and electron-irradiated (Nos. 1A and 1B) Cz-Si samples (Fig. 2) demonstrated that the shape of equal-intensity lines on them is typical for the case of circular dislocation loops with the $\langle 111 \rangle$ Burgers vector orientation [15]. The radii of these loops R_L were estimated using the measured reciprocal space maps and their cross sections (Figs. 2 and 3). For the irradiated samples, they turned out to be two fold less than for the initial crystal. The concentration n_L of these (large) dislocation loops in the irradiated samples proved to be significantly (by an order of magnitude and more) larger as compared to the concentration in the initial sample (see table). An estimate for large spherical oxygen precipitates was obtained simultaneously with the estimate for the sizes of large loops. The size of the precipitates was $R_p \approx 1 \mu\text{m}$ in all samples. Their concentration n_p after irradiation of the samples significantly increased (table).

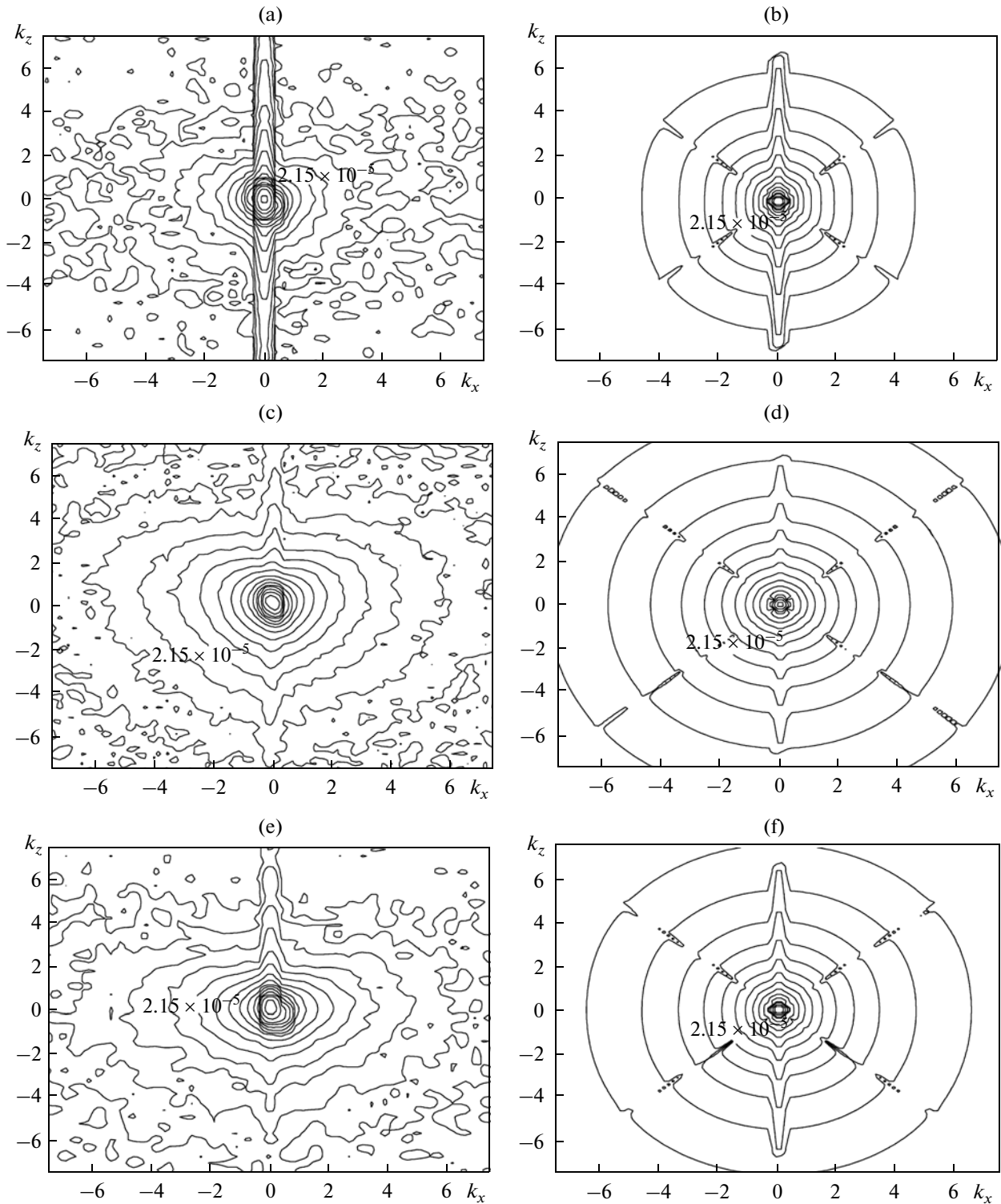


Fig. 2. (c, e) Measured and (d, f) calculated reciprocal space maps of the initial (No. 1) and electron-irradiated (Nos. 1A and 1B) Cz-Si samples; 333 reflection and $\text{CuK}\alpha_1$ radiation.

Final values of the characteristics of large dislocation loops and precipitates were obtained after introducing small dislocation loops into the combined

treatment. In our case, small dislocation loops with radii of several nanometers give a significant contribution at the far tails of the RC for all studied samples

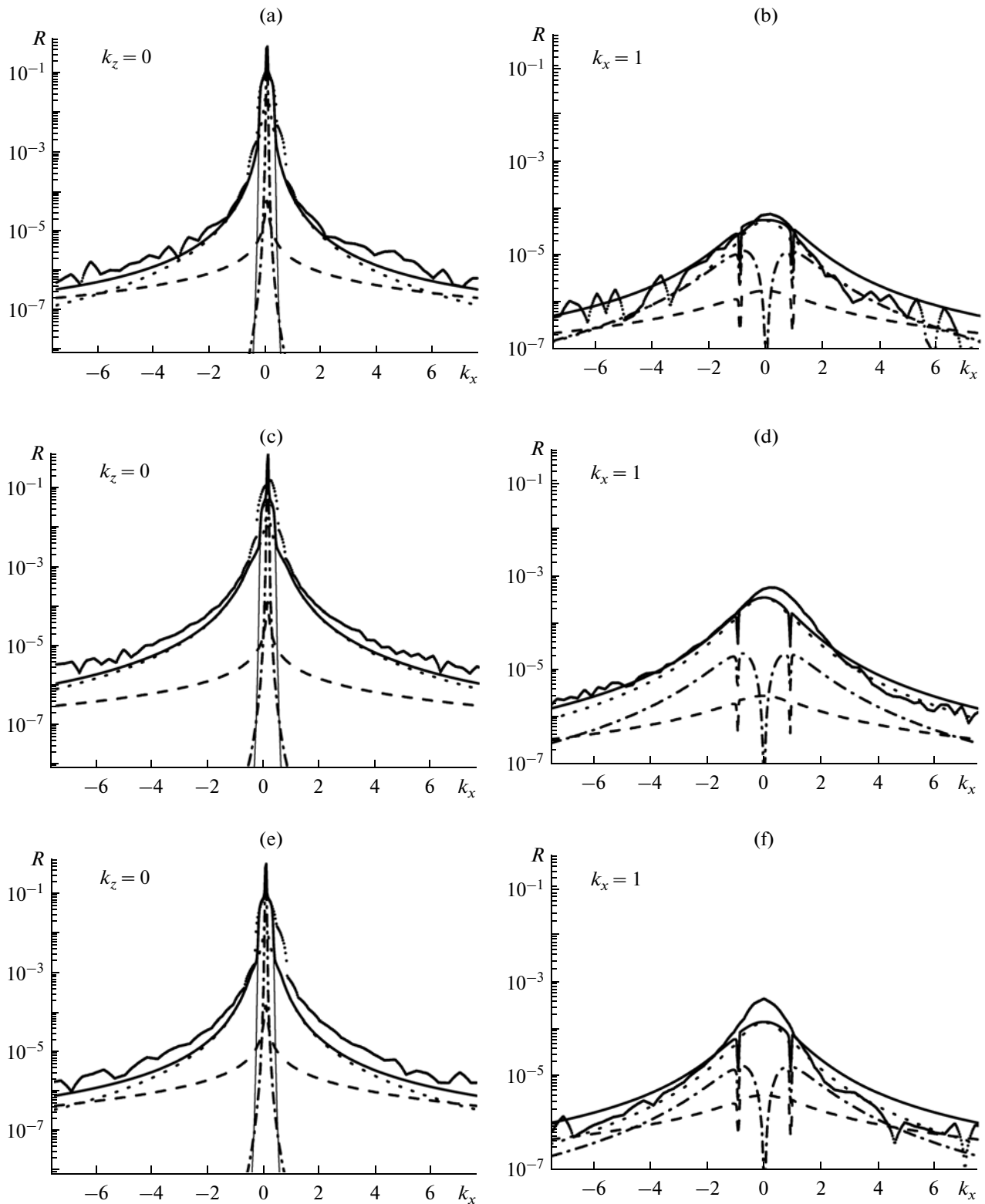


Fig. 3. (c, e) Transverse and (d, f) longitudinal cross sections of the reciprocal space map (Fig. 2). The measured and calculated profiles are represented by markers and the thick solid line. The calculated profile consists of a coherent component and contributions to the DS intensity from small and large dislocation loops, as well as from oxygen precipitates (thin solid, dashed, dotted, and dot-dashed lines, respectively).

(Fig. 4); at the same time, their contribution is negligible in the TCD diffraction profiles (compare Figs. 3 and 4). As can be seen from the table, the concentrations of small dislocation loops in the irradiated samples are approximately two fold smaller than in the initial crystal.

In spite of the fact that there is a certain size distribution of defects in the crystal, one can nevertheless assert that the dominant contributions are those from defects with values of radii obtained as a result of fitting. These values seem to account for centers of the corresponding size distributions of defects.

When being irradiated with high-energy electrons, the defect structure in the bulk of the silicon crystal varies under the influence of two factors. The first of them is the appearance of radiation defects, first of all, vacancies and interstitial silicon atoms. The second one is the increasing crystal temperature which accelerates diffusion processes. As can be seen from the results of diagnostics (table), these factors resulted in considerable changes of the growth defect characteristics in both the irradiated silicon samples as compared to the initial crystal.

The mobility of dissolved oxygen atoms increases in silicon samples irradiated with high-energy electrons due to an increase in the temperature (to approximately 1000°C for the chosen irradiation parameters), and the oversaturated solid solution of oxygen in silicon continues to decompose. As a consequence, the concentration of oxygen precipitates increased in both the irradiated silicon samples. At the same time, the considerable redistribution of sizes and concentrations occurs due to growth defects interaction: on the one hand, with radiation defects (interstitial silicon atoms and vacancies); on the other hand, with interstitial silicon atoms that are emitted by the growing oxygen precipitates to decrease strain at their boundary with the matrix. As this takes place, the concentration of small dislocation loops decreases with a certain increase in their size and the concentration of large loops increases with a significant decrease in their radii (see table).

Duplication of the dose of high-energy electron irradiation only leads to a small constriction of the tails of the diffuse background in the diffraction pattern (Figs. 2–4). This, as it is seen from the table, corresponds to a small increase in the radius and decrease in the concentration of large dislocation loops which make the main contribution to the DS intensity in the aforesaid angular range. Such disproportional changes in the defect structure of irradiated silicon samples with a significant (twofold) increase in the irradiation dose are probably caused by the fact that the sizes and concentrations of the ensemble of growth microdefects and secondary radiation defects reach their thermodynamically equilibrium values at even smaller doses. A further increase in the electron irradiation dose has no significant effect on the change in the microdefect parameters. Another probable cause of

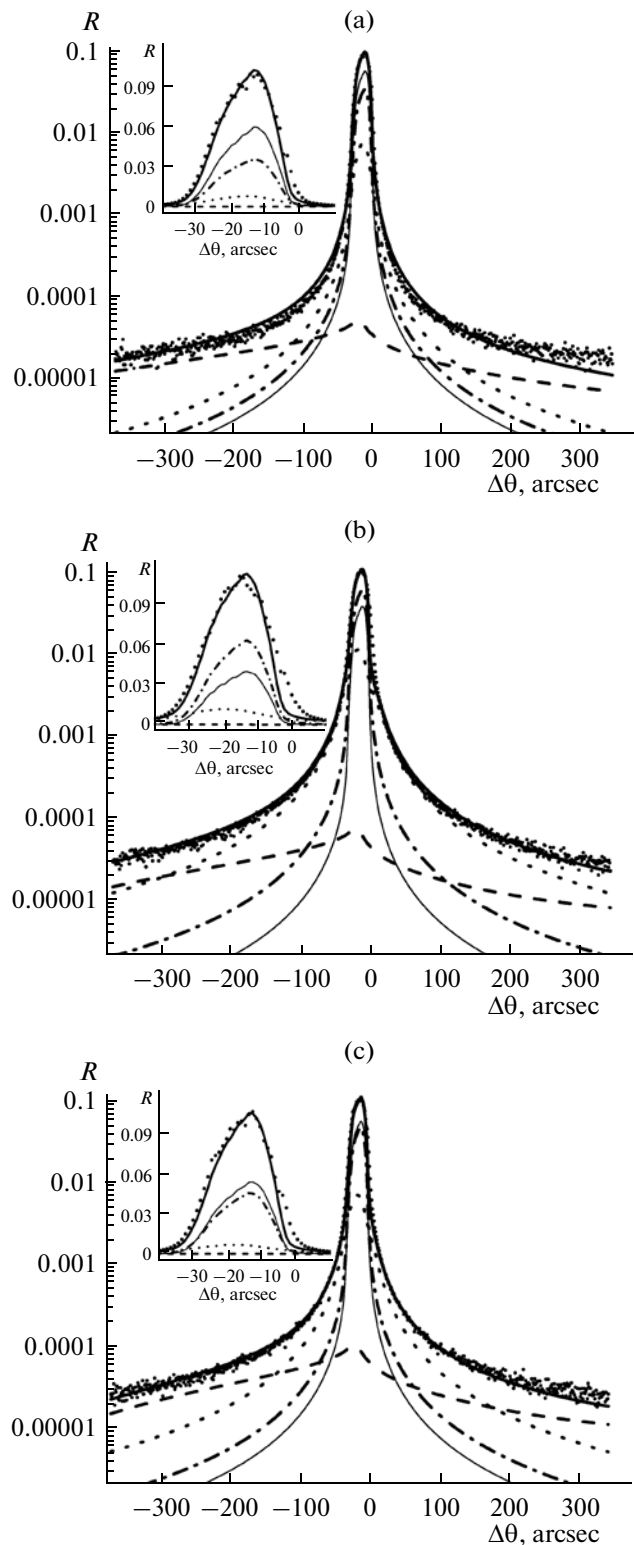


Fig. 4. Experimental and theoretical RCs (markers and thick lines) for the (a) initial and (b, c) electron-irradiated Cz-Si samples Nos. 1A and 1B; 333 reflection and $\text{Cu}K_{\alpha 1}$ radiation. Other lines are as in Fig. 3. Central parts of the RCs are shown in the inserts.

Characteristics of dislocation loops (radius R_L and concentration n_L) and oxygen precipitates (R_p and n_p) in the initial (No. 1) and electron-irradiated (Nos. 1A and 1B) Cz-Si samples

Sample	Dislocation loops		Oxygen precipitates		R factors for the RCs	
	R_L , μm	n_L , cm^{-3}	R_p , μm	n_p , cm^{-3}	R , %	R_w , %
No. 1	0.002	1.15×10^{16}	1	7.5×10^6	9	18
	0.15	3.3×10^{11}				
No. 1A	0.003	5×10^{15}	1	1.25×10^7	12	11
	0.065	1×10^{13}				
No. 1B	0.003	5×10^{15}	1	9×10^6	10	10
	0.07	3.5×10^{12}				

such disproportional changes in the defect structure can be the transition of the defect-formation process to the self-oscillating mode under irradiation. This mode is characterized by cyclic variations in the parameters of defects in small ranges [19].

CONCLUSIONS

The obtained results demonstrate the possibility of increasing the unambiguity of the quantitative diagnostics of complex defect structures in imperfect single crystals owing to the combined treatment of RCs and reciprocal space maps. In particular, for silicon single crystals irradiated with high-energy electrons, this combined treatment with using analytical formulas of the statistical dynamical theory of X-ray diffraction in imperfect crystals made it possible to find the quantitative characteristics of large and small defects.

The obtained quantitative information about the interaction between point defects and microdefects ensured more correct analysis of the influence of high-energy electron irradiation on single crystal imperfections and, in particular, made it possible to take into account for the first time the role of growth microdefects in the transformations of primary and secondary radiation defects in silicon.

ACKNOWLEDGMENTS

The work was supported by the State Target Scientific-Technical Program "Nanotechnologies and Nanomaterials" (project No. 3.6.3.13-7/11-D).

REFERENCES

- M. Mikelsen, E. V. Monakhov, G. Alfieri, et al., Phys. Rev. B **72**, 195207 (2005).
- N. Inoue, H. Ohyama, Y. Goto, and T. Sugiyama, Physica B **401–402**, 477 (2007).
- A. Khan, J. Gou, M. Imazumi, and M. Yamaguchi, Appl. Phys. Lett. **91**, 043503 (2007).
- M. D'Amico, F. Messina, M. Cannas, et al., Phys. Rev. B **79**, 064203 (2009).
- A. P. Antipenko, G. L. Bochek, V. V. Gann, et al., Pov-erkhnost', No. 4, 41 (2006).
- V. Neimash, M. Kras'ko, A. Kraitchinskii, et al., Phys. Status Solidi A **201**, 509 (2004).
- O. V. Feklisova, A. N. Tereshchenko, E. A. Shteinman, et al., J. Surf. Invest. **1**, 398 (2007).
- V. V. Uglov, N. T. Kvasov, Yu. A. Petukhov, et al., J. Surf. Invest. **6**, 67 (2012).
- L. Fedina, A. Gutakovskii, A. Aseev, et al., Phys. Status Solidi A **171**, 147 (1999).
- K. Karsten and P. Ehrhart, Phys. Rev. B **51**, 10508 (1995).
- A. Pillukat, K. Karsten, and P. Ehrhart, Phys. Rev. B **53**, 7823 (1996).
- V. V. Dovganyuk, N. V. Litvinchuk, V. V. Slobodjan, and I. M. Fodchuk, Proc. SPIE **7008**, 1B1 (2008).
- V. B. Molodkin, S. I. Olikhovskii, E. N. Kislovskii, et al., Phys. Status Solidi B **227**, 429 (2001).
- S. I. Olikhovskii, V. B. Molodkin, E. N. Kislovskii, et al., Phys. Status Solidi B **231**, 199 (2002).
- V. B. Molodkin, S. I. Olikhovskii, E. G. Len, et al., Phys. Status Solidi A **206**, 1761 (2009).
- V. B. Molodkin, S. I. Olikhovskii, E. N. Kislovskii, et al., Phys. Rev. B **78**, 224109 (2008).
- V. Holý, U. Pietsch, and T. Baumbusch, *High-Resolution X-Ray Scattering from Thin Films and Multilayers*, Springer Tracts in Modern Physics, Vol. 149, Springer Telos, Berlin, Heidelberg, 1999).
- A. Borghesi, B. Pivac, A. Sassella, and A. Stella, J. Appl. Phys. **77**, 4169 (1995).
- P. A. Selishchev, *Self-Organization in Radiation Physics* (Regulyar. Khaotich. Dinamika, Inst. Komp. Issled., Izhevsk, 2008) [in Russian].

Translated by A. Nikol'skii